Supplementary Information

Possibilities and Limitations of AFM-IR to Detect Nanoplastic Particles in the Atmosphere

Nico Kummer*[1], Stefan Horender[2], Tero S. Kulmala[3], Konstantina Vasilatou[2], Christoph Hüglin[4], Ralf Kaegi*[1]

[1] *Particle Laboratory, Department of Process Engineering, Eawag (Swiss Federal Institute of Aquatic Science and Technology), Ueberlandstrasse 133, 8600 Dübendorf, Switzerland*

[2] *Particles and Aerosols Laboratory, Federal Institute of Metrology METAS, Lindenweg 50, 3003 Bern, Switzerland*

[3] *Laboratory for Transport at Nanoscale Interfaces, Empa (Swiss Federal Laboratories for Materials Science and Technology), Ueberlandstrasse 129, 8600 Dübendorf, Switzerland*

[4] *Laboratory for Air Pollution and Environmental Technology, Empa (Swiss Federal Laboratories for Materials Science and Technology), Ueberlandstrasse 129, 8600 Dübendorf, Switzerland*

* corresponding authors

contact NK: n.kummer@hotmail.com; contact RK: ralf.kaegi@eawag.ch

Contents:

Supplementary Methods

M1: Fabrication of the octagon silicon substrates

Single-side polished, undoped Silicon (Si)-wafers with a thickness of 525 µm and a native oxide layer were cut into regular octagons (d ~ 3 mm) with a Trotec Speedmarker 300 laser cutter (λ = 1064 nm, pulse duration 110 nm). First, the polished side of the wafer was spin-coated (4000 rpm, 40 s) with a layer of protective photoresist (AZ1505, MicroChemicals GmbH) followed by a soft-bake at 110 °C for 1 minute on a hot plate. The wafer was cut with the (non-coated and non-polished) backside facing up using a cutting speed of 300 mm/s, a power setting of 80% and 250 passes. As a result, the octagon pieces were fully detached from the surrounding silicon. The protective resist layer was removed by ultrasonicating the octagons in acetone for a few minutes followed by ultrasonication in isopropanol for a few minutes and drying with a nitrogen gun. Finally, the octagons were cleaned in a plasma chamber (PVA TePla; 50 sccm Ar + 50 sccm O_2, P=100 W) for 5 min. The cleanliness and the dimensions of the octagons were verified with an optical microscope (Keyence VHX-7000) (Fig. S12).

M2: Synthetic aerosol generation using the PALMA facility

Protocols for the generation of each model aerosol are shown below. The number-based geometric mean diameter (GMD_{mob}) and geometric standard deviation (GSD_{mob}) of the mobility particle size distributions, and the number concentration were determined for each model aerosol using a Scanning Mobility Particle Sizer (SMPS) comprising an Electrostatic Classifier (Series 3080, DMA 3081, 3 L min^{-1} sheath air, TSI Incorporated, USA) and a Condensation Particle Counter (CPC, 3776 low flow 0.3 L min^{-1}, TSI Incorporated, USA) operated with the commercial software AIM 10.3 (TSI Incorporated, USA). This instrument had been traceably calibrated with respect to particle size and number concentration. Particle size distributions are reported in Fig. S1-S5.

Inorganic salt: Aqueous solutions of 1.15 g of ammonium nitrate (>99%, Acros Organics, Slovakia) and of 1.4 g of ammonium sulfate (>99.5%, Acros Organics; Netherlands) in 70 g ultrapure water were nebulized with a AGK 2000 atomizer (PALAS, Germany). The aerosol had a GMD_{mob} of 135 nm and a GSD_{mob} of 1.9.

Mineral dust particles (ISO A2 test dust, 72% SiO2, DMT, USA) were dispersed with a rotating-brush generator (RBG 1000, PALAS, Germany). The aerosol had a GMD_{mob} of 50 nm and GSD_{mob} of 2.0. For sample S14, dust particles were dispersed using the atomizer AGK 2000 (PALAS, Germany).

Soot particles were generated with a miniCAST 5301 burner (Jing Ltd., Switzerland) using propane as fuel. The aerosol had a GMD_{mob} of 120 nm and a GSD_{mob} of 1.6. The particles were then aged by ozonolysis of α-pinene (>97%, Sigma Aldrich, Switzerland) using a prototype micro smog chamber. The size distribution had a GMD_{mob} of 180 nm and a GSD_{mob} of 1.2.

PS particles were nebulized using an aerosol generator, model ATM221 (TOPAS, Germany). The aerosol was subsequently passed through an Aerodynamics Aerosol Classifier (Cambustion, UK) to remove most of the residuals.

For sample 16 only, mineral dust (1 g) was added to the salt solution listed above, and the aerosol was generated using the same atomization method.

Supplementary Figures

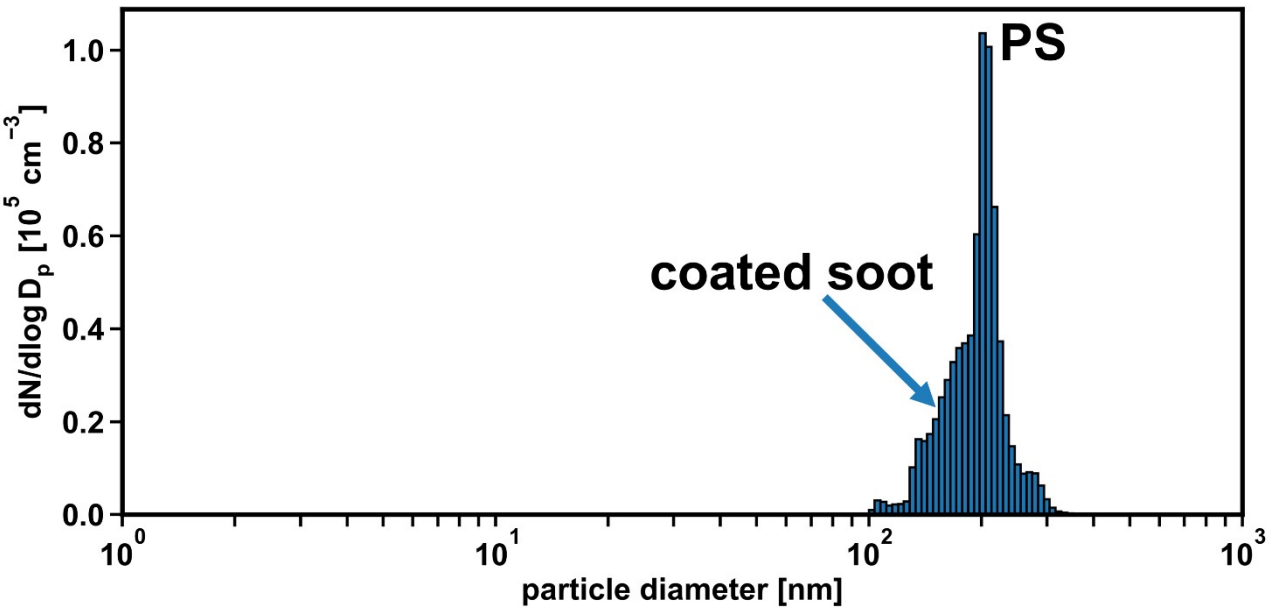

***Fig. S1**: Size distribution derived from scanning mobility particle sizer (SMPS) measurements of the synthetic aerosol consisting of polystyrene particles (200 nm) and aged soot (sample 13)*

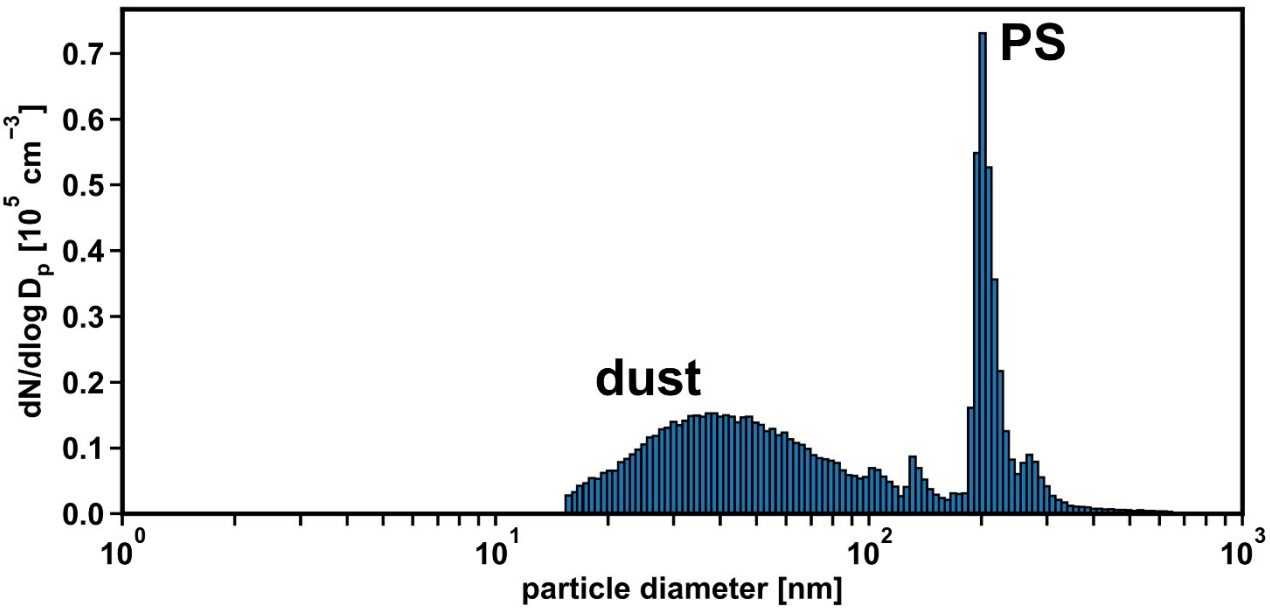

***Fig. S2**: Size distribution derived from scanning mobility particle sizer (SMPS) measurements of the synthetic aerosol consisting of polystyrene particles (200 nm) and mineral dust (sample 14).*

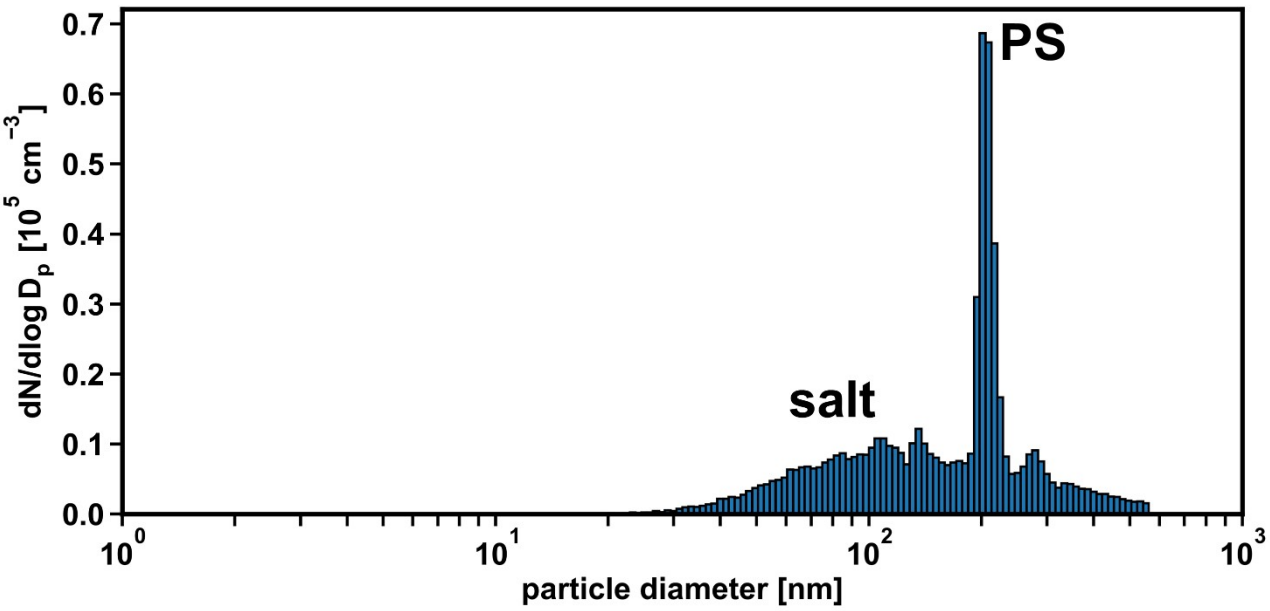

***Fig. S3**: Size distribution derived from scanning mobility particle sizer (SMPS) measurements of the synthetic aerosol consisting of polystyrene particles (200 nm) and ammonium sulfate/nitrate (sample 15)*

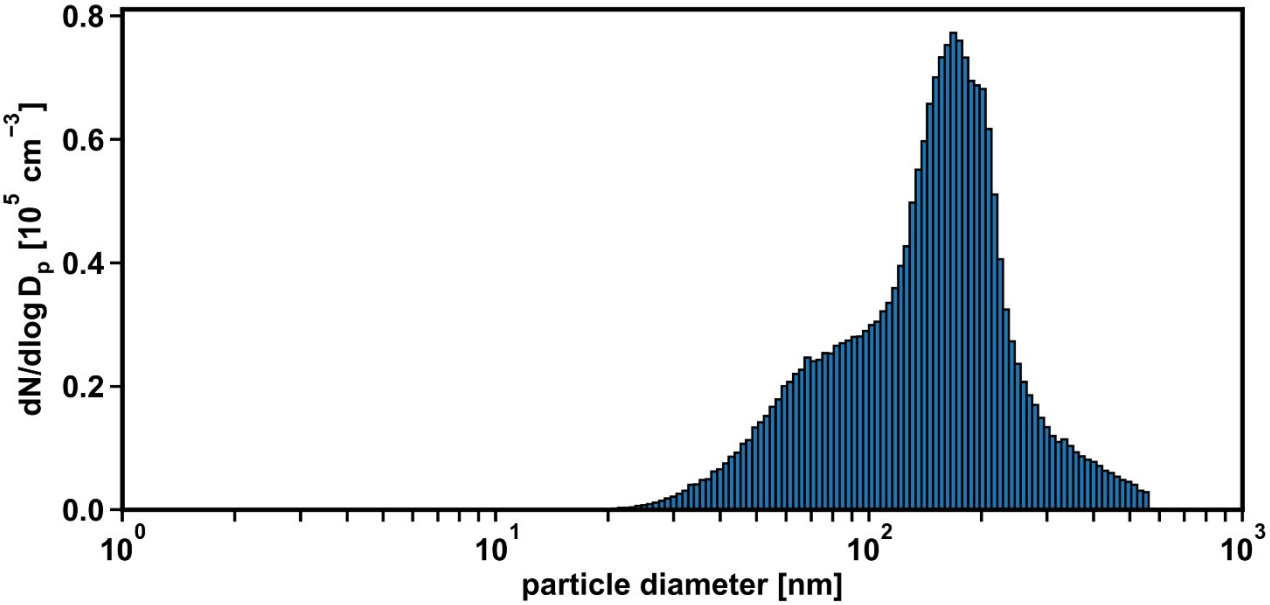

***Fig. S4**: Size distribution derived from scanning mobility particle sizer (SMPS) measurements of the synthetic aerosol consisting of polystyrene particles (200 nm), ammonium sulfate/nitrate, aged soot and mineral dust (sample 16).*

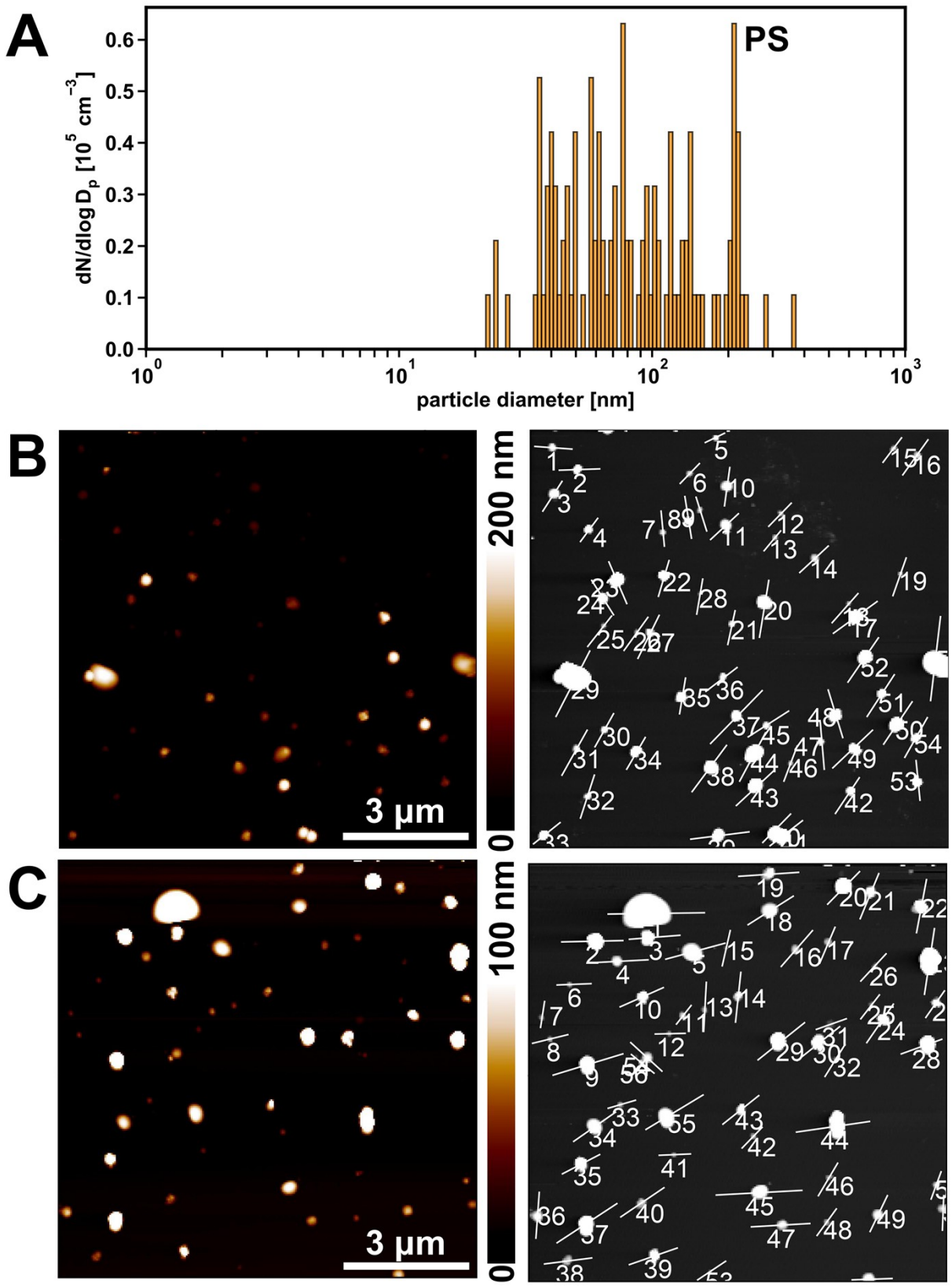

Fig. S5: *Particle size distribution (A) based on the atomic force microscopy-infrared spectroscopy (AFM-IR) height data (extracted from images shown in B and C) of the synthetic aerosol consisting of polystyrene (PS) particles (200 nm), ammonium sulfate/nitrate, aged soot and mineral dust (sample 16).*

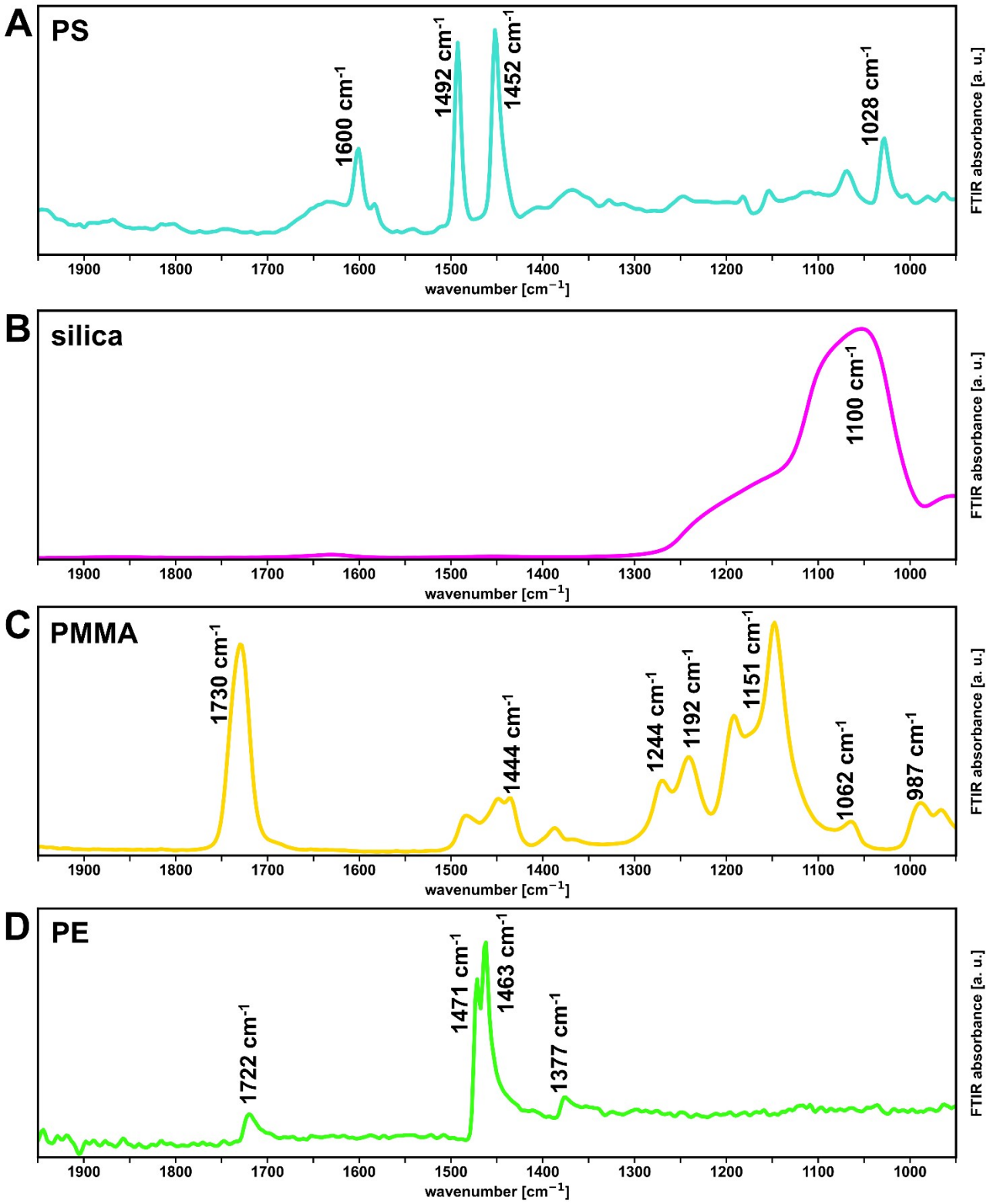

***Fig. S6**: Attenuated total reflection (ATR) – Fourier transform infrared (FTIR) spectra of (A) polystyrene (PS), (B) silica, (C) poly(methyl methacrylate) (PMMA) and (D) polyethylene (PE).*

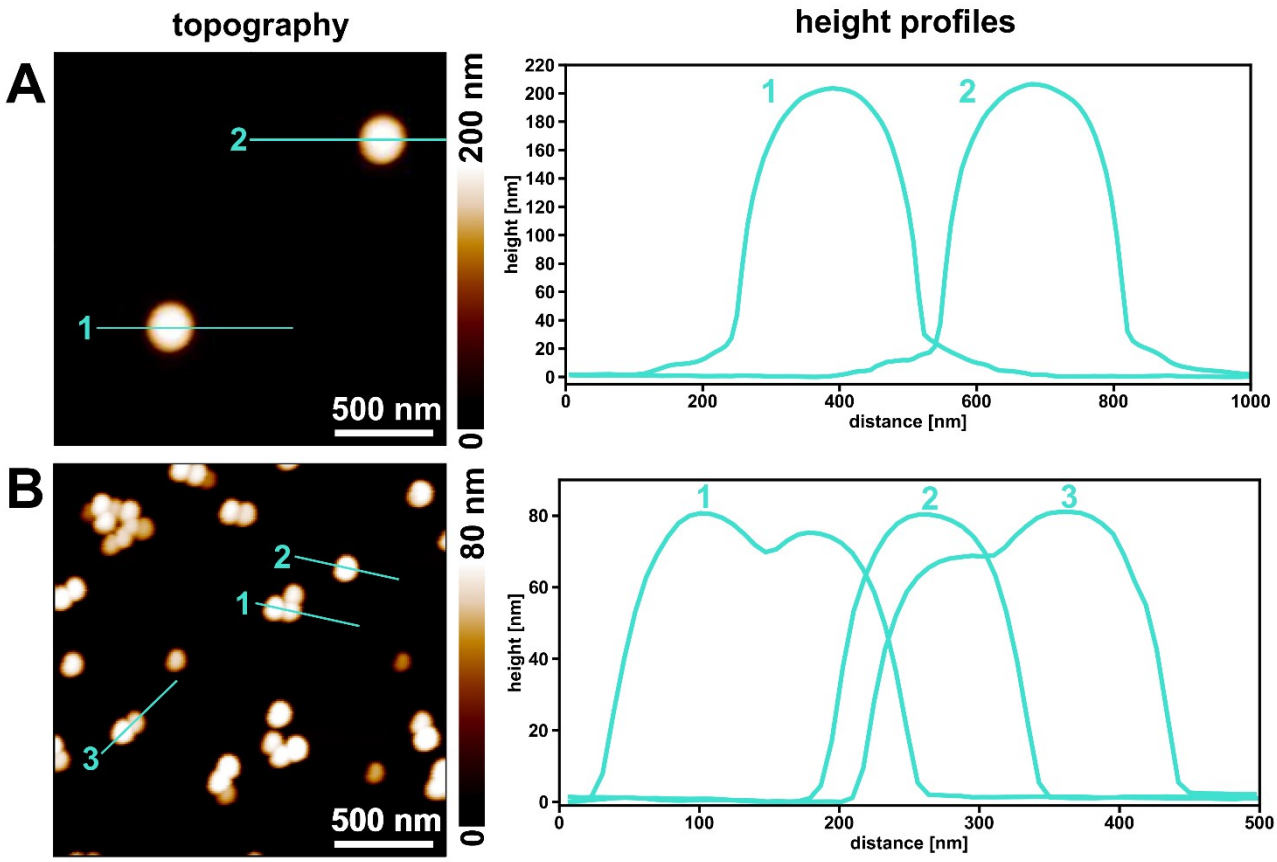

Fig. S7: *Atomic force microscopy-infrared spectroscopy (AFM-IR) topography images replotted from Fig. 2 with height profiles along the enumerated lines for (A) 200 nm polystyrene (PS) (sample 4) particles and (B) 80 nm PS particles (sample 3).*

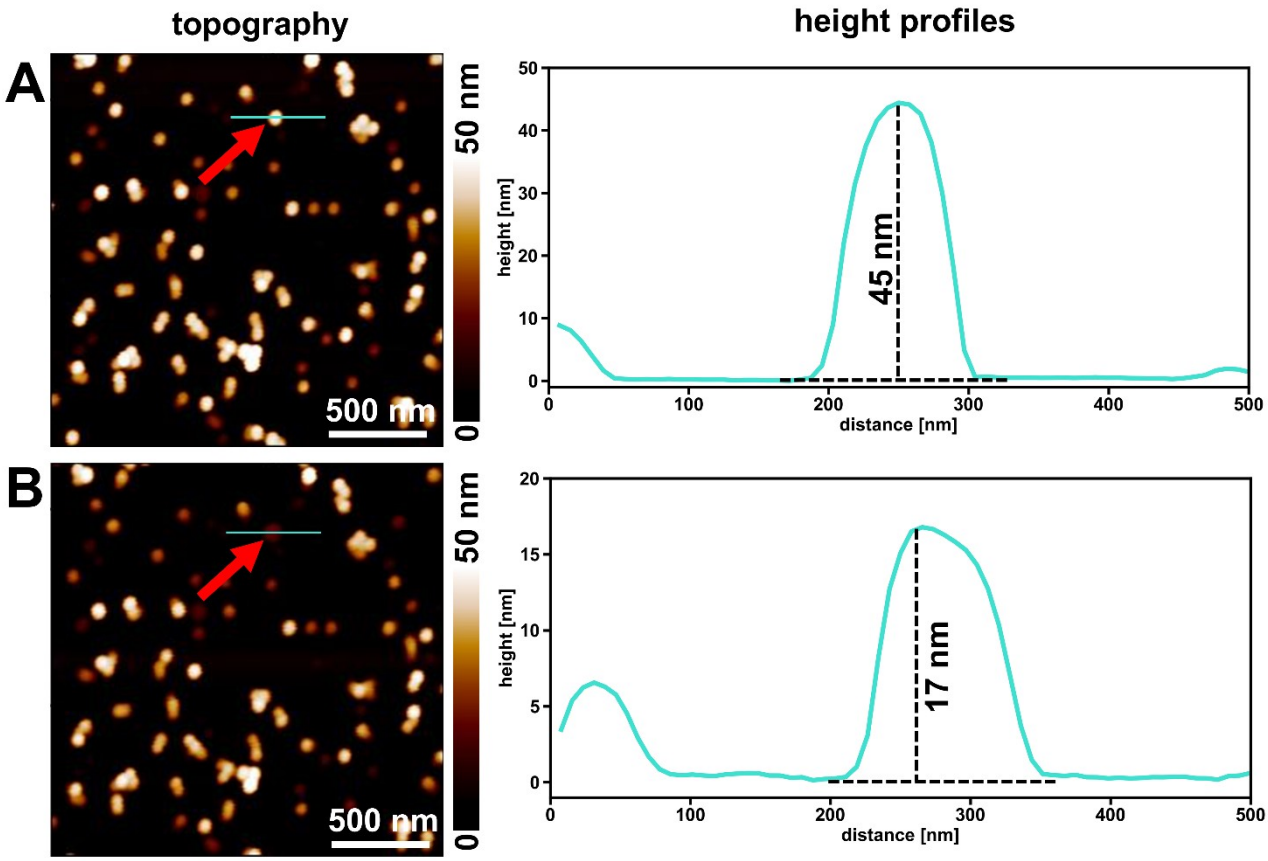

***Fig. S8**: Atomic force microscopy-infrared spectroscopy (AFM-IR) topography images with height profiles along the lines for 50 nm polystyrene (PS) particles (sample 2). (A) before and (B) after acquiring a spectrum from the particle indicated with the red arrow.*

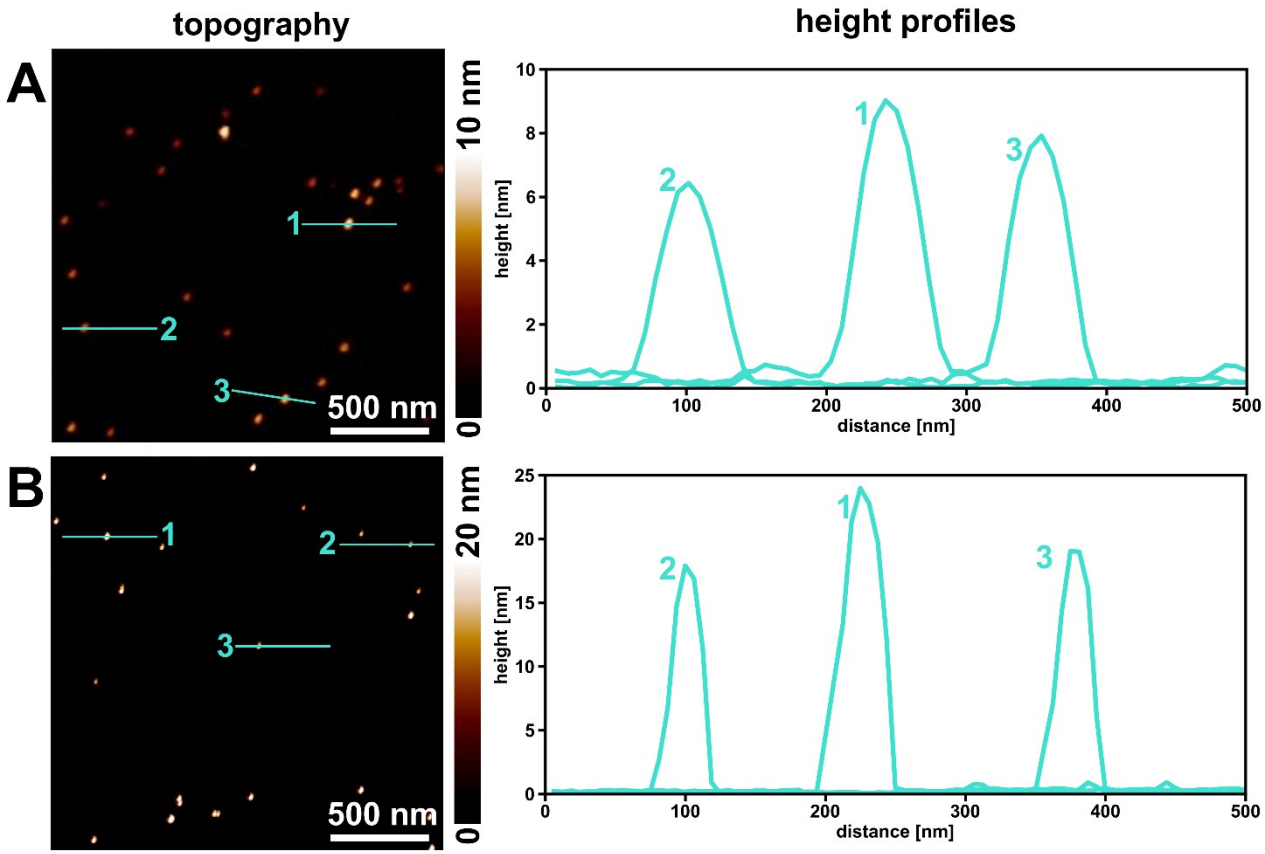

***Fig. S9**: (A) Atomic force microscopy-infrared spectroscopy (AFM-IR) topography image replotted from Fig. 2D with height profiles along the enumerated lines for 20 nm polystyrene (PS) particles (sample 1). (B) AFM topography image with height profiles along the enumerated lines for 20 nm PS particles deposited on a mica substrate. Data acquired with a Bruker Dimension Icon operated in peak-force tapping based ScanAsyst mode (force controlled).*

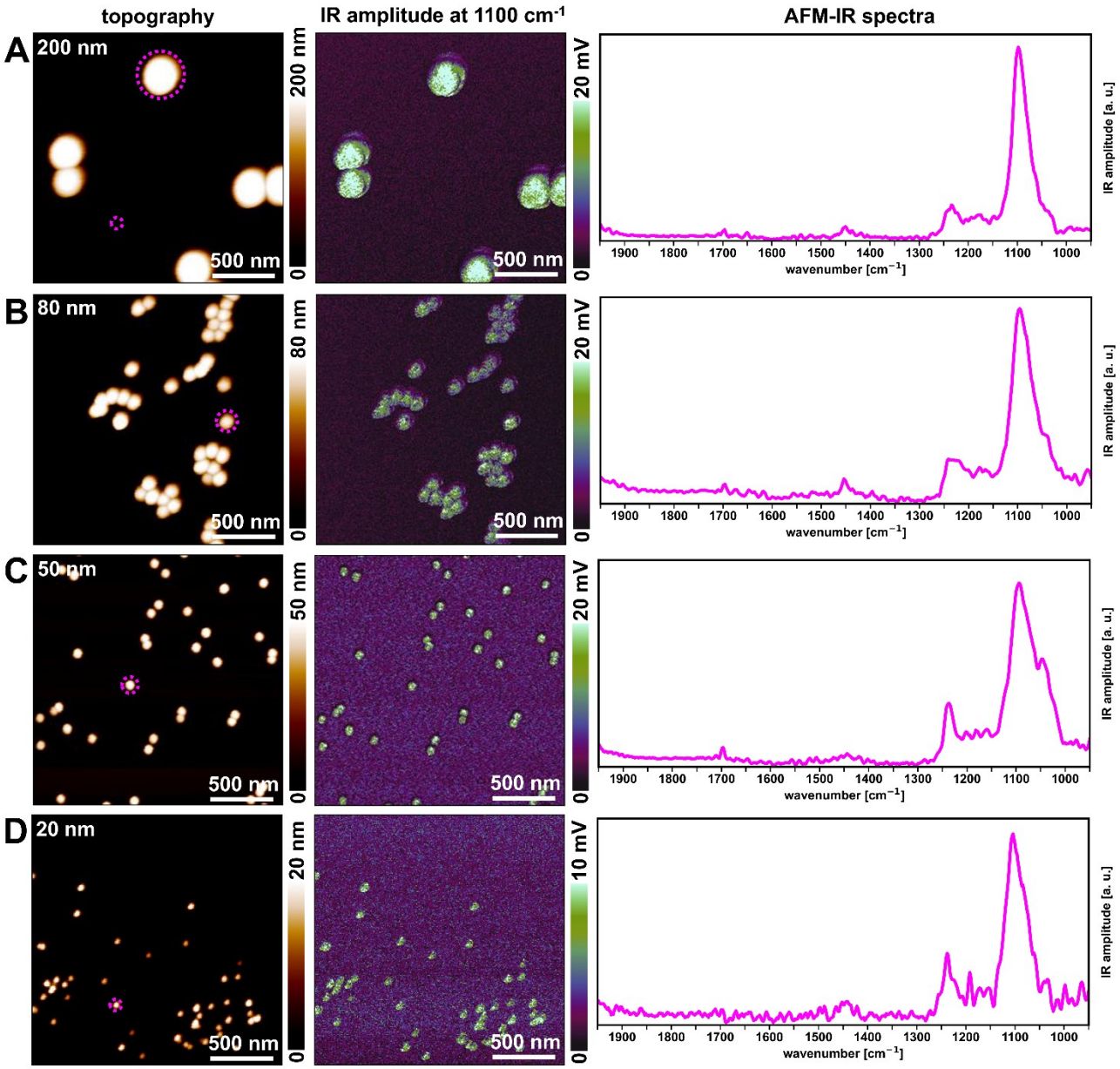

***Fig. S10**: Atomic force microscopy-infrared spectroscopy (AFM-IR) topography images, IR amplitude images at 1100 cm $^{-1}$ (Si-O stretching vibration of silicates) and AFM-IR spectra of silica particles of various sizes deposited on Si-wafers: (A) 200 nm (sample 8), (B) 80 nm (sample 7), (C) 50 nm (sample 6), and (D) 20 nm (sample 5). The IR spectra were recorded in the center of the encircled silica particles.*

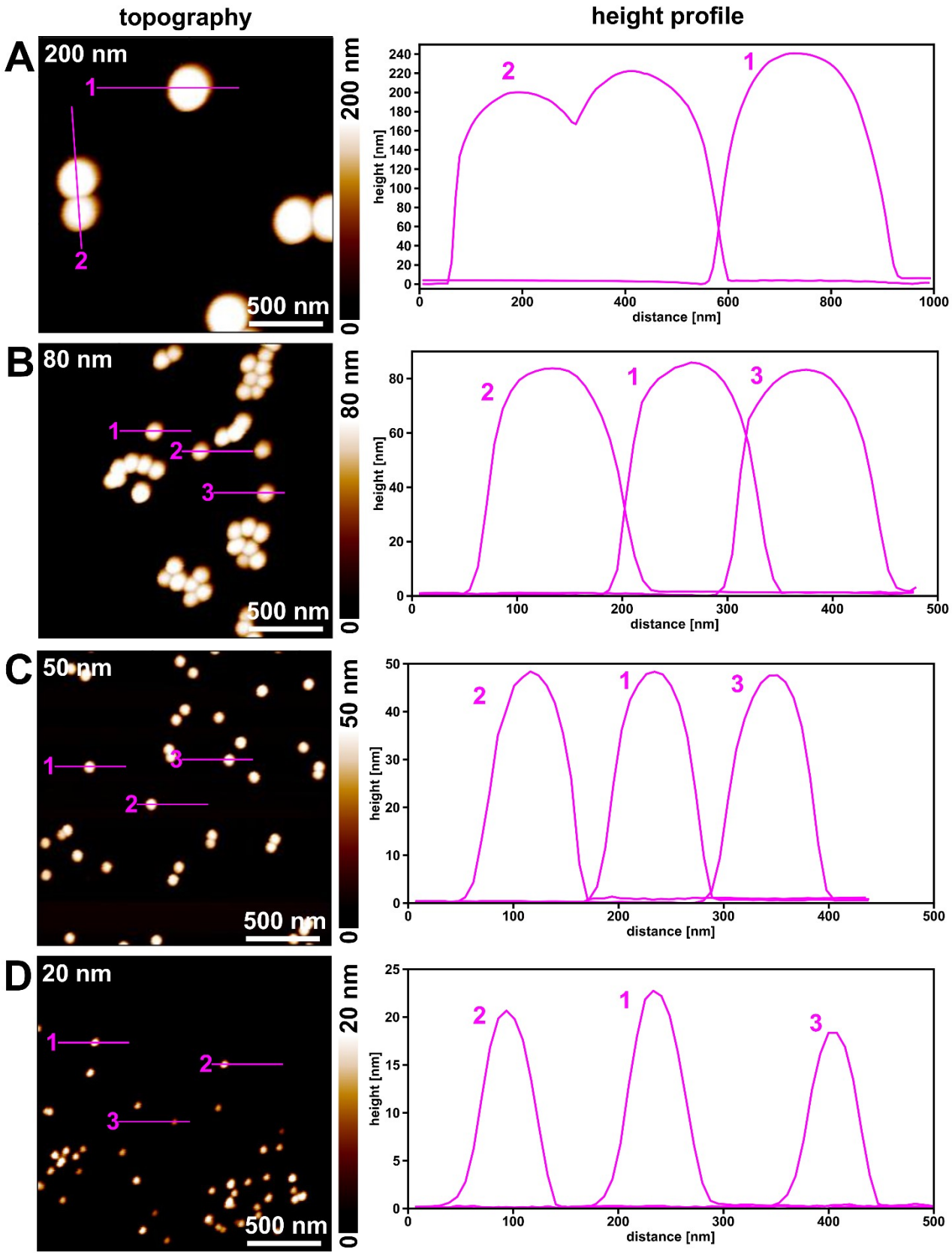

***Fig. S11**: Atomic force microscopy-infrared spectroscopy (AFM-IR) topography images replotted from Fig. S10 with height profiles along the enumerated lines for (A) 200 nm silica particles (sample 8), (B) 80 nm silica particles (sample 7), (C) 50 nm silica particles (sample 6) and (D) 20 nm silica particles (sample 5).*

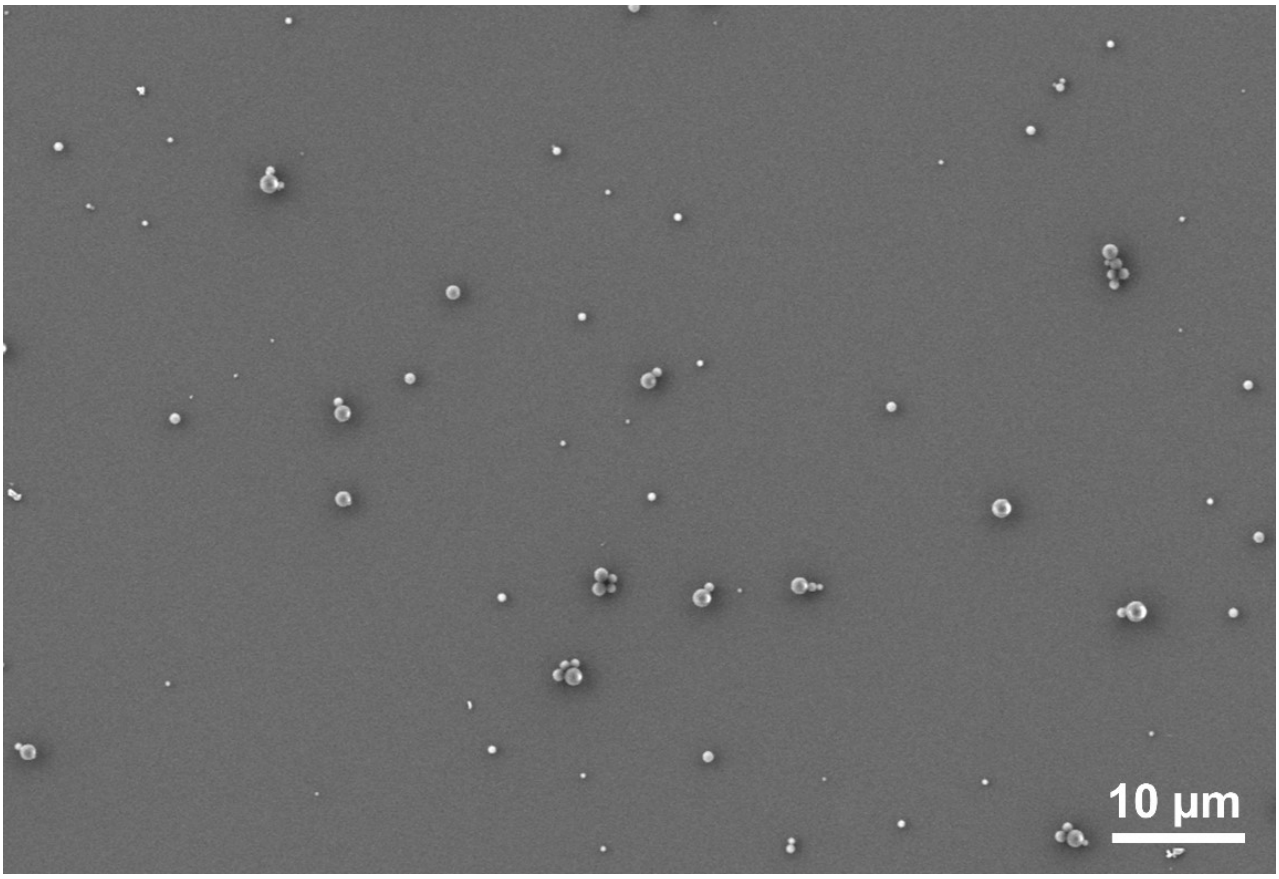

***Fig. S12**: Secondary electron image of polyethylene (PE) particles deposited from a polydisperse suspension on a Si-wafer (sample 10), showing the presence of particles smaller than 1 µm. The suspension was sedimented overnight to remove larger PE particles. The smallest particles with a diameter of 200 nm were used to test the size limit of detection of the atomic force microscopy-infrared spectroscopy (AFM-IR) for PE. The low particle concentrations of PE (at or close to 200 nm) hampered the production of meaningful mixtures of PE and other particles.*

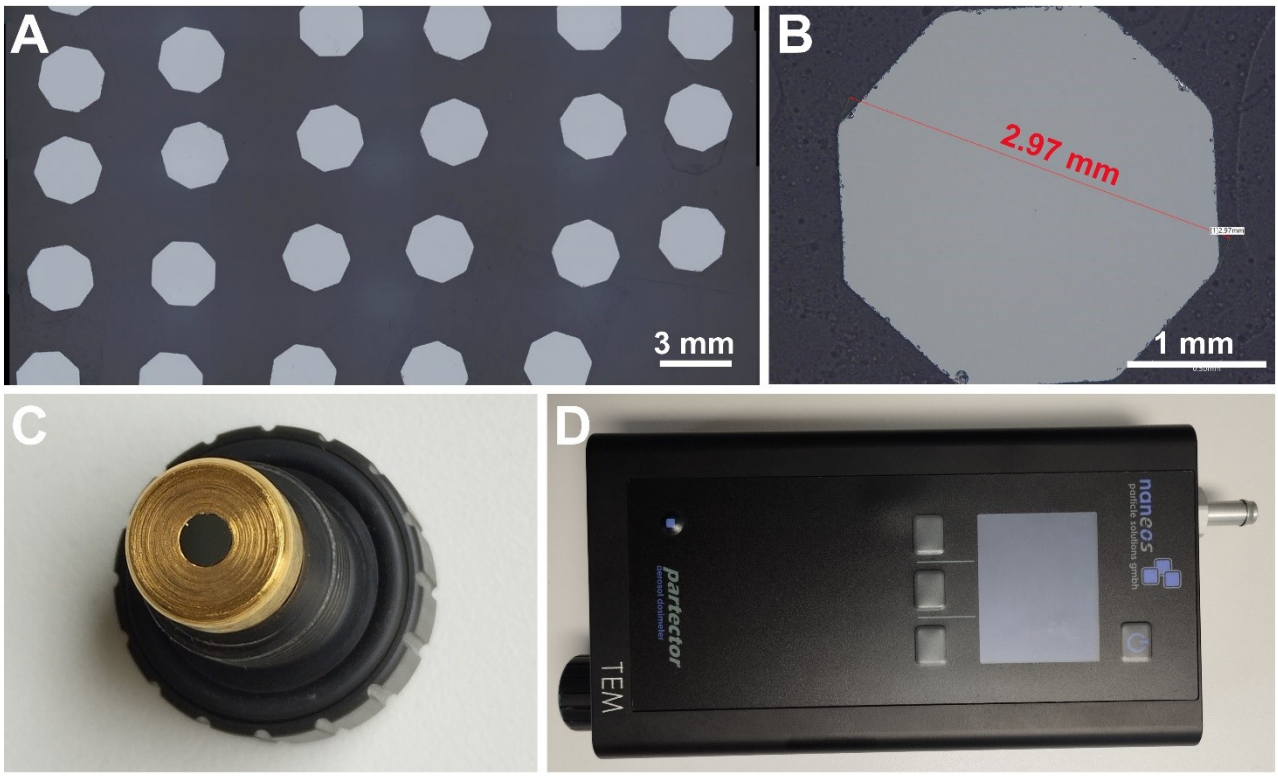

***Fig. S13**: (A)Characterization of the laser-cut silicon (Si)-wafer octagons by optical microscopy. (B) Dimension of the laser-cut octagon. (C) Grid holder for the PartectorTEM with inserted Si-wafer octagon. (D) PartectorTEM with grid holder screwed in and ready for sampling.*

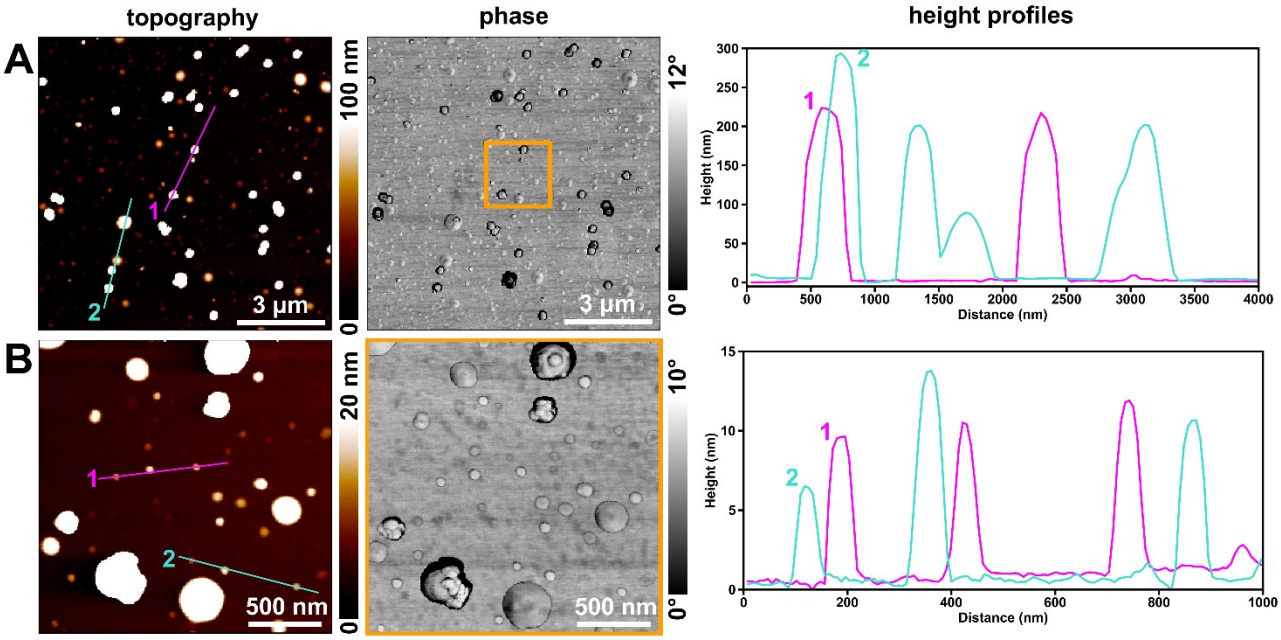

***Fig. S14**: (A) Atomic force microscopy-infrared spectroscopy (AFM-IR) topography and phase images corresponding to Fig. 7 (ambient aerosol deposited on Si-wafer previously spiked with 200 nm polystyrene (PS) particles (sample 17)) with height profiles along the enumerated lines. (B) AFM topography (rescaled to 20 nm) and phase images with height profiles along the enumerated lines. The orange box indicates the area in A that is shown enlarged in B.*

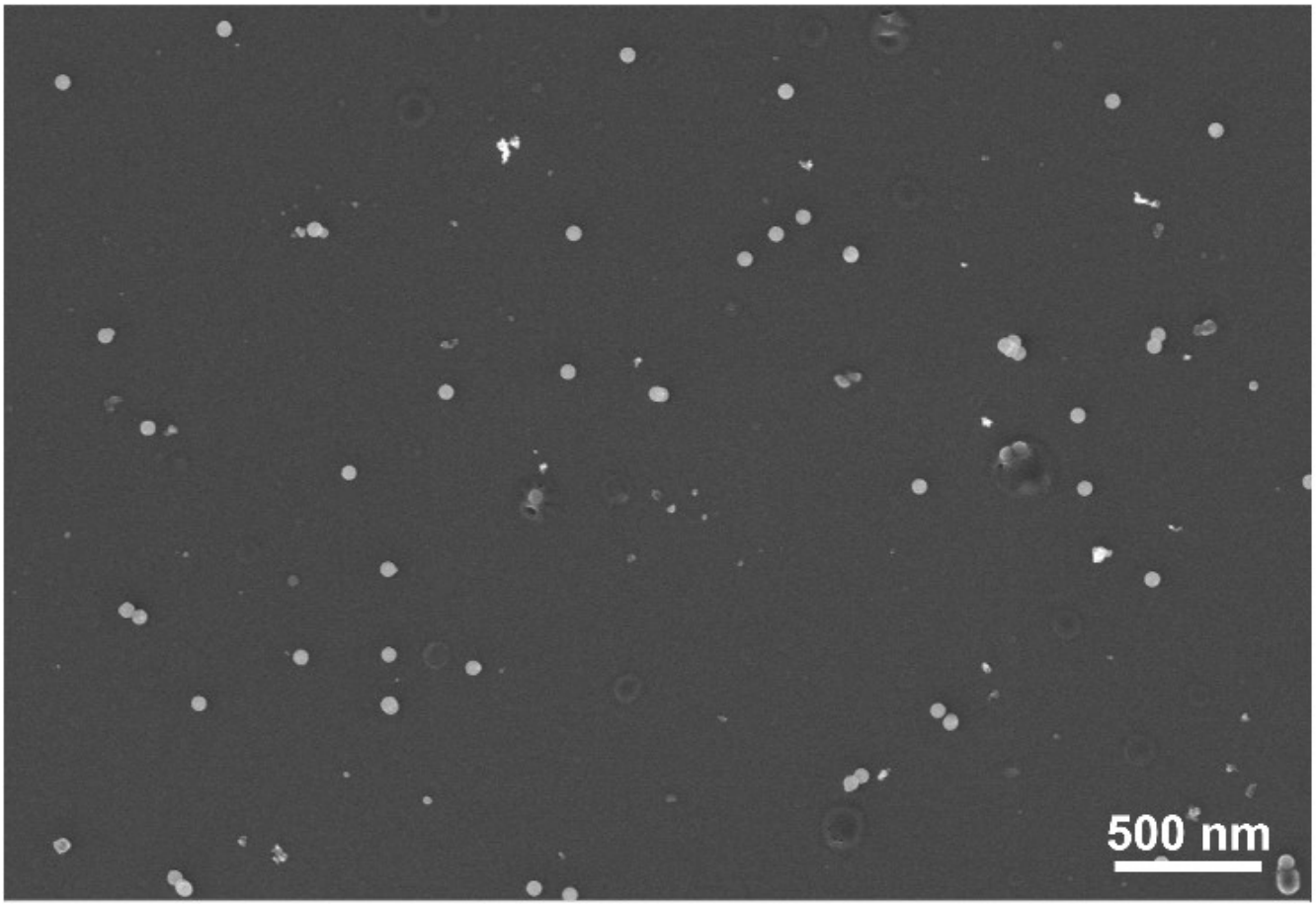

Fig. S15*: Secondary electron image of sample 17, demonstrating the even electrostatic precipitation of spiked polystyrene (PS) particles (spherical) and ambient aerosol particles.*

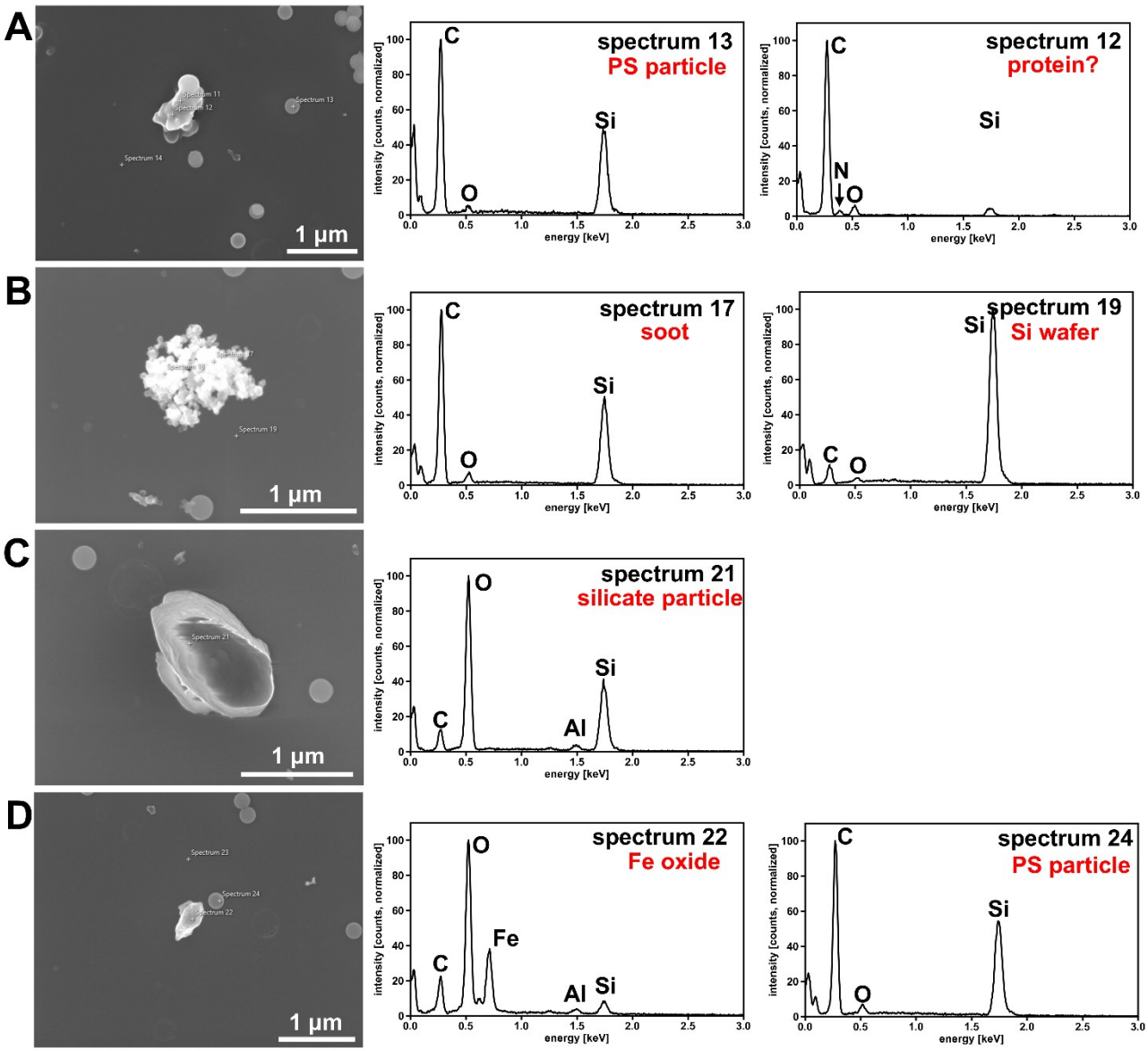

***Fig. S16**: Secondary electron images (left column) and corresponding energy dispersive X-ray (EDX) spectra (middle and right columns) of selected particles from the PS spiked sample collected from ambient air (sample 17). Based on their elemental spectra and their morphology, the particles were identified as PS and protein (A), soot and the Si-wafer background (B), silicate dust particle (C), and iron oxide and PS particle (D).*

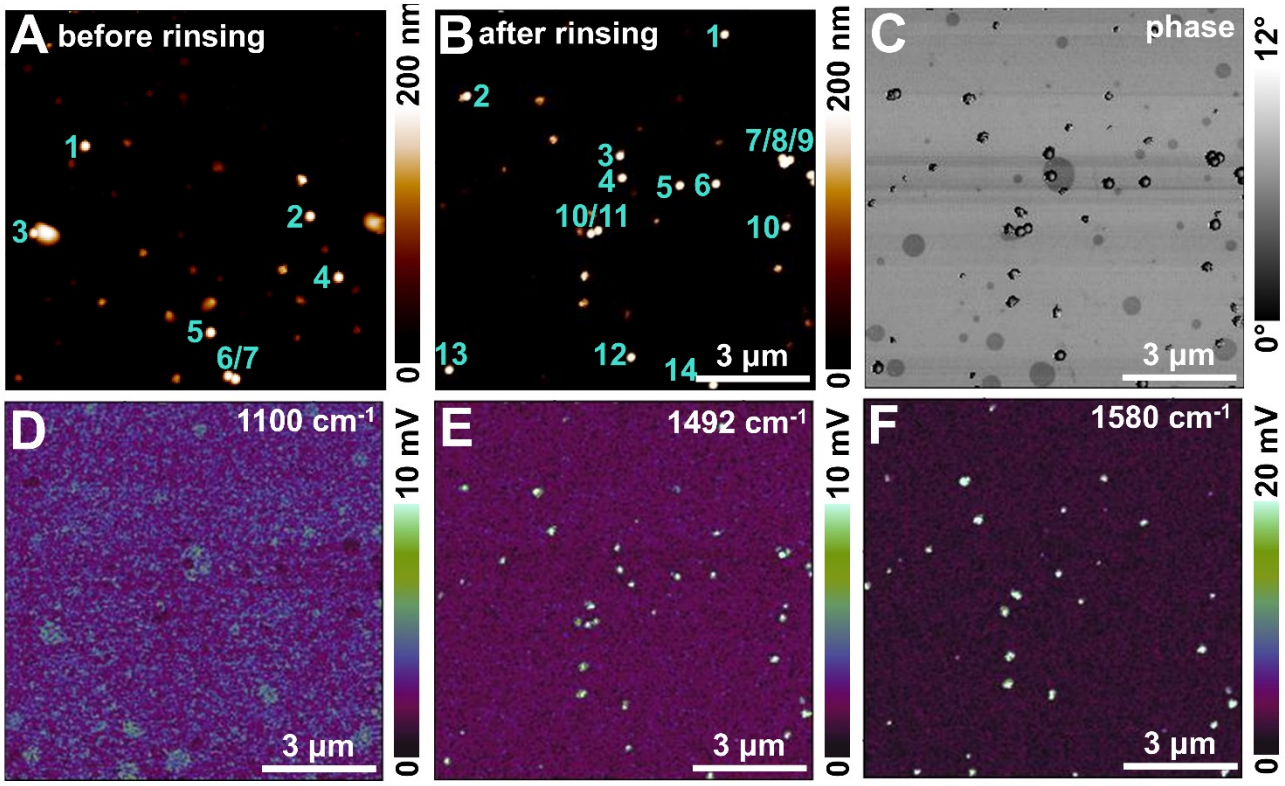

***Fig. S17**: Synthetic aerosol (sample 16) with 200 nm PS before (A) and after (B-F) rinsing (5 µL of water deposited on the Si-wafer and blown off by dry nitrogen gas after 1 min). The numbers in the topography images before and after rinsing refer to the count of PS particles, which remained on the Si-wafer after the rinsing step. Note the traces of sulfate visible in the phase image (C) and in the IR amplitude image at 1100 cm^{-1} (D). IR amplitude images at 1492 cm^{-1} (E) and 1580 cm^{-1} (F) confirm that PS particles and soot remain on the Si-wafer.*

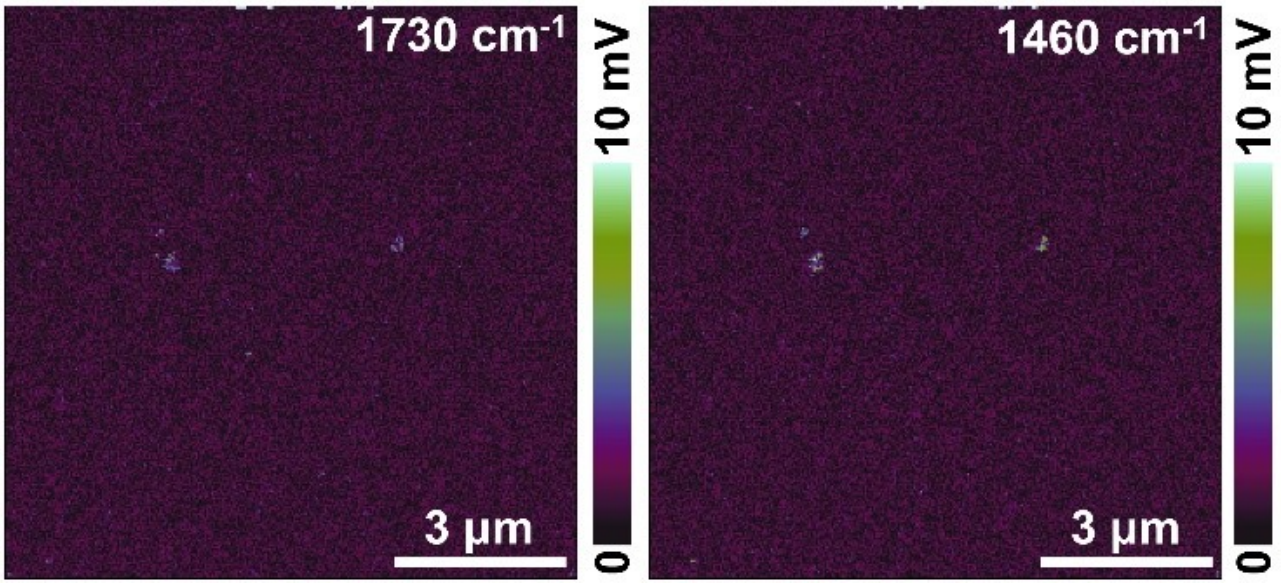

***Fig. S18**: Atomic force microscopy-infrared spectroscopy (AFM-IR) amplitude images at 1730 cm^{-1} (C=O stretching vibration of ester group, left), and at 1460 cm^{-1} (C-H bending vibration of methylene group, right) to detect polyethylene/polypropylene and polyesters, respectively. A weak signal from soot particles is visible, which is caused by the broad IR adsorption of soot at around 1580 cm^{-1}.*

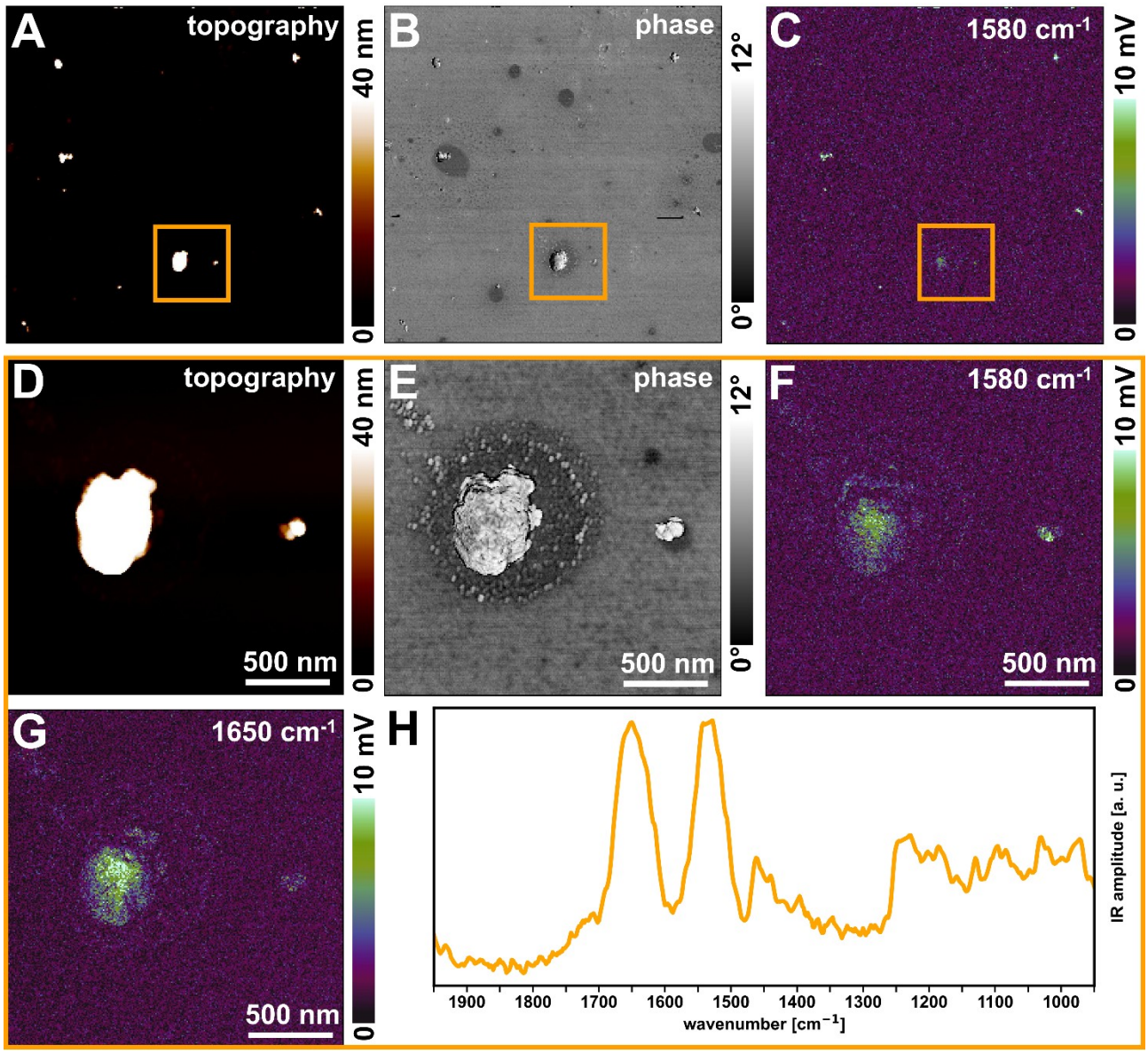

***Fig. S19**: AFM-IR topography (A, D), phase (B, E) and IR amplitude images (C, F, G) of a protein particle detected in the ambient aerosol sample. (D-F) are detailed AFM-IR images of the area indicated by the orange box in (A-C). The signal at 1580 cm^{-1} (C, F) was lower than expected for a soot particle of this size, but the intensity was higher at 1650 cm^{-1} (G) which is typical for the amide I band of proteins. AFM-IR spectrum of the particle showing the typical amide I (1650 cm^{-1}) and II (1550 cm^{-1}) absorption bands (H).*